Effects of La concentration on the structural and magnetic properties of $BiFeO_3$ nanoparticles

LIU ZHAO-JUN[a,b,*], ZHAO JIAN-GUO[a,b,*], ZHANG WEI-YING[a,b], LIU SHI-JIANG[a,b]
[a] *School of Physics and Electronic Information, Luoyang Normal College, Henan, Luoyang 471022, PR China*
[b] *Luoyang Key Laboratory of Laser Spectroscopy Technology, Henan, Luoyang 471022, PR China*

$Bi_{1-x}La_xFeO_3$ (x= 0.05, 0.1, 0.15, 0.2, and 0.25) nanoparticles were synthesized by sol-gel method, and the effects of La content on the structure and magnetic properties were investigated. X-ray diffraction and Raman analysis showed that the structure of La-doped $BiFeO_3$ was transformed from a rhombohedral to a orthorhombic with the increase of La content. This was also accompanied by an increase in the magnetization up to x=0.20 followed by a reverse trend at higher doping levels. The enhanced ferromagnetism might be attributed to the antiferromagnetic core and ferromagnetic surface of the nanoparticles, the increasing of canting angle, and the structural distortion. When the dopant concentration up to x=0.25, the decreased ferromagnetism might be attributed to the decreased of ferromagnetic component of canted Fe sublattice.

(Received March 18, 2013; accepted March 13, 2014)

Keywords: $BiFeO_3$, Nanoparticles, Raman, Magnetic properties

1. Introduction

Multiferroic materials, exhibiting simultaneously the magnetic and ferroelectric order, have been widely studied in recent years, due to their abundant physics and potential applications in the sensors, data storage, spin valve devices, actuators, ultra-high speed telecommunication devices, and spintronics [1-5]. Out of all the multiferroic materials studied so far, $BiFeO_3$ is a single phase multiferroic, among the few reported so far, and it has great potential for practical applications exhibiting ferroelectricity with high Curie temperature (T_C~1103 K), and antiferromagnetic properties below the Neel temperature(T_N~643 K) [6-9]. Much effort has been paid to improve the magnetization in $BiFeO_3$ to get a sizable response to the application of magnetic field [10, 11].

There are many reports on the enhancement in the magnetization of $BiFeO_3$ in the bulk, thin films, and nanoparticles, on Bi-site substitution by selected trivalent rare-earth (RE) and divalent ions, or on Fe-site substitution by transition metal ions. For example, substitution of Bi^{3+} with rare-earth elements, such as Ho^{3+}, Gd^{3+}, or Sm^{3+}, resulted in remarkable improvement of the ferroelectric and ferromagnetic of $BiFeO_3$, which could possibly lead to enhanced magnetoelectric effect [12-14]. On the other hand, Fe, the smaller B-site cation, has been substituted by elements such as Co, Ni, or Mn, which resulted in an increase in the polarization but also led to a substantial increase in the coercive field [15-17].

In this paper, we prepared La doped $BiFeO_3$ nanoparticles by a sol-gel method followed by a rapid thermal annealing process. The crystal structures, morphologies, and magnetic properties were investigated in detail. It is well known that La, belongs to the lanthanides and the ionic radius of La^{3+} (1.06 Å) is smaller than that of Bi^{3+} (1.20 Å), which can lead to large lattice distortion and enhance the magnetic properties.

2. Experiments

2.1 Sample preparation

$Bi_{1-x}La_xFeO_3$ (x= 0.05, 0.1, 0.15, 0.2, and 0.25) nanoparticles were prepared by sol-gel method with $Fe(NO_3)_3$•$9H_2O$, $La(NO_3)_3$•$6H_2O$, $Bi(NO_3)_3$·$5H_2O$, 2-methoxyethanol, acetic acid, citric acid as the starting materials. First $Bi(NO_3)_3$•$9H_2O$ and $La(NO_3)_3$•$6H_2O$ were dissolved in acetic acid under constant magnetic stirring for 2 h. Then $Fe(NO_3)_3$•$9H_2O$, 2-methoxyethanol and citric acid were added to the solution. After continuous stirring for 2h, the solution was aged for 1 day, dried at 80 ℃for 48 h and grinded into powders. At last, the powder was sintered at 750 ºC for 2h in air, and then subsequently cooled rapidly to room temperature. A series of samples of La-doped $BiFeO_3$ nanoparticles ($Bi_{1-x}La_xFeO_3$) with x= 0.05, 0.10, 0.15, 0.20, and 0.25 were prepared by adopting the same procedure as mentioned above.

2.2 Characterization

Powder X-ray diffraction (XRD) patterns were recorded on Bruker D8 ADVANCE with Cu K_α radiation (λ=1.54 Å). Raman scattering spectra were recorded on a

JY-HR800 Raman spectrometer using an Ar^+ laser (514.5 nm) as the excitation line. The transmission electron microscopy (TEM) and the corresponding selected area electron diffraction (SAED) pattern were collected on Tecnai F30 transmission electron microscope. Variable-temperature magnetization measurements under a magnetic field of 1000 Oe (1 Oe = 79.577 A/m) and under both zero-field-cooled (ZFC) and field-cooled (FC) conditions were performed on a Quantum Design SQUID MPMS XL-7 (SQUID) from 300 K down to 5 K. The dc hysteresis loops were collected on the same SQUID in magnetic fields from 50000 to -50000 Oe at 5 and 300 K, respectively.

3. Results and discussion

Fig. 1 (a) shows the XRD patterns of the La-doped $BiFeO_3$ nanoparticles. The peaks corresponding to a standard JCPDS pattern of $BiFeO_3$ were found in all samples. Peak intensity ratios suggest a polycrystalline behavior with good crystallinity. With increasing of La concentration, two features should be noted in Fig. 1. One is that except characteristic peaks of $BiFeO_3$, other peaks (indicated by star symbols) appear at $Bi_{1-x}La_xFeO_3$ ($x \geq 0.10$) samples, which are attributed to the new phase of $LaFeO_3$. Another feature is that a closer comparison of XRD patterns of the nanoparticles with varying dopant concentrations (x=0.05-0.25) revealed shifts in the peak positions and gradual reduction in the peak splitting. Fig. 1 (b) and (c) shows the profiles of (111) and (110) peaks which clearly show merger of split peaks into a single peak at x=0.15. It is found that from x=0.15 to x=0.25, only single peak is present for each diffracting plane with no apparent splitting. At the same time, no systematic peak absences are observed. A gradual lattice distortion and finally a structural transition from rhombohedral to orthorhombic structure are confirmed in these ceramics as the doping content x is increasing from 0.05 to 0.25. This classification is consistent with the early reports on Gd doped $BiFeO_3$ ceramics implying that the structural phase transition starts at approximately the composition of x = 0.1 [18]. Furthermore, when increasing La concentration to 0.15, the contribution of rhombohedral phase decreases, while the contribution of orthorhombic phase increases. The phase transition from rhombohedral to orthorhombic symmetry is attributed to the structural distortion resulting from the incorporation of La^{3+} ions into the lattice of $BiFeO_3$, because the ionic radius of La^{3+} is smaller than that of Bi^{3+}. Although minor impurity of $Bi_{25}FeO_{40}$ and $LaFeO_3$ marked by asterisk and #, respectively, could be detected in Fig. 1(a), it is not ferromagnetic in nature at room temperature and thus has no contribution to the ferromagnetic property as observed in the $Bi_{1-x}La_xFeO_3$ samples.

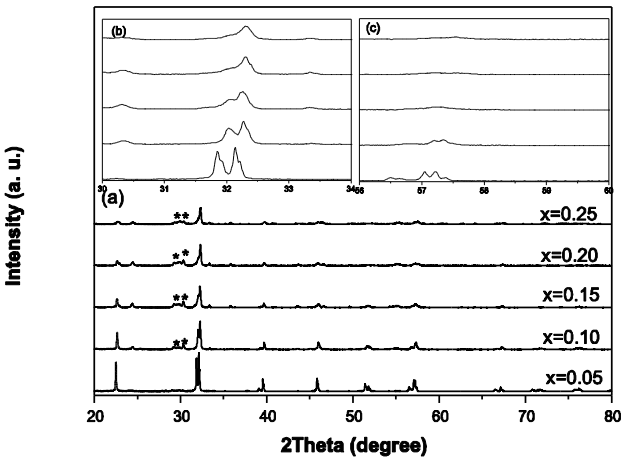

Fig. 1. XRD patterns of $Bi_{1-x}La_xFeO_3$ (x=0.05, 0.10, 0.15, 0.20, 0.25) nanoparticles sintered at 750 °C for 2 h. Inset: (b) the magnified XRD patterns in the vicinity of 2θ around 32 degrees; (c) the magnified XRD patterns in the vicinity of 2θ around 57 degrees.

Since Raman scattering spectra are sensitive to atomic displacements, the evolvement of Raman normal modes with increasing x may provide valuable information about the lattice properties, structural phase transitions, and spin-phonon coupling. Fig. 2 shows the measured Raman scattering spectra of $Bi_{1-x}La_xFeO_3$ (x=0.05, 0.10, 0.15, 0.20, 0.25) samples at room temperature. It has been reported that the Raman active modes of the rhombohedral R3c $BiFeO_3$ can be summarized using the following irreducible representation: $\Gamma=4A_1+9E$ [19-21]. For $BiFeO_3$ nanoparticles with rhombohedral R3c symmetry, there are eleven normal modes, including E-1, A_1-1, A_1-2, and A_1-3 modes with strong scattering intensities at 76, 140, 172, and 220 cm^{-1}, respectively, The subsequent six peaks at 278, 339, 370, 474, 530, and 610 cm^{-1} can be assigned as E-2, E-3, E-4, E-5, E-6, and E-7 modes, respectively. The peak at 425 cm^{-1} that can be assigned as A_1-4 mode is too weak to be detected in our $Bi_{0.95}La_{0.05}FeO_3$ sample and peak at 113 cm^{-1} that can be assigned as E-1 mode is overlap with 140 cm^{-1} mode. However, with the increasing of La doping concentrations to 0.10, E-1, A_1-1, A_1-2, and A_1-3 modes, which are governed by Bi-O convalent bonds is red shift indicating that the La is entering into the Bi-site of $BiFeO_3$. When the La concentration is increasing to 0.15, the E-1, A_1-1, and A_1-2 modes nearly disappear, indicating the phase transition happened at this concentration. Moreover, several new peaks is observed, which may result from $LaFeO_3$ phase in the compounds. Such peaks have also been reported to exist in $RFeO_3$ (R=Gd, Dy et al.). These results are agreement with the XRD results.

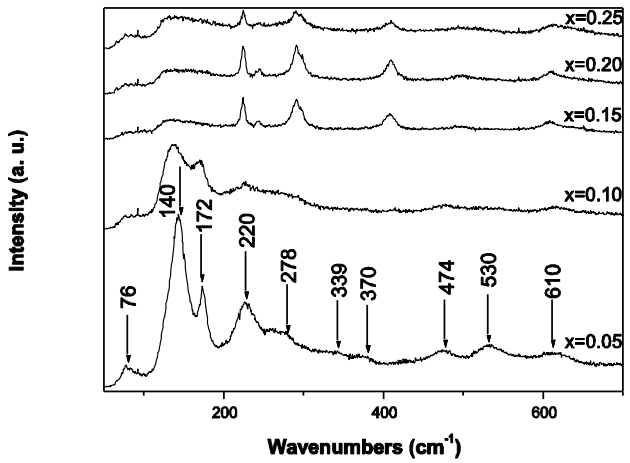

Fig. 2. Raman spectra of $Bi_{1-x}La_xFeO_3$ (x=0.05, 0.10, 0.20, 0.25) nanoparticles sintered at 750 °C for 2 h.

A typical TEM image of the 10 % La-doped $BiFeO_3$ nanoparticles is shown in Fig. 3 (a). The average crystallite size is about 25 nm, close to that estimated from XRD patterns with Scherrer equation. Fig. 3 (b) is a corresponding high-resolution TEM (HRTEM) image of 10 % La-doped $BiFeO_3$ nanoparticles. The regular spacings of the observed lattice is 0.278 nm, which are consistent with the (110) crystal planes of rhombohedral $BiFeO_3$ crystal. SAED (selected area electron diffraction) pattern taken for the 10 mol% La-doped $BiFeO_3$ NPs [Fig. 3(c)] shows the presence of sharp diffraction spots indicating the formation of well developed, highly crystalline nanoparticles.

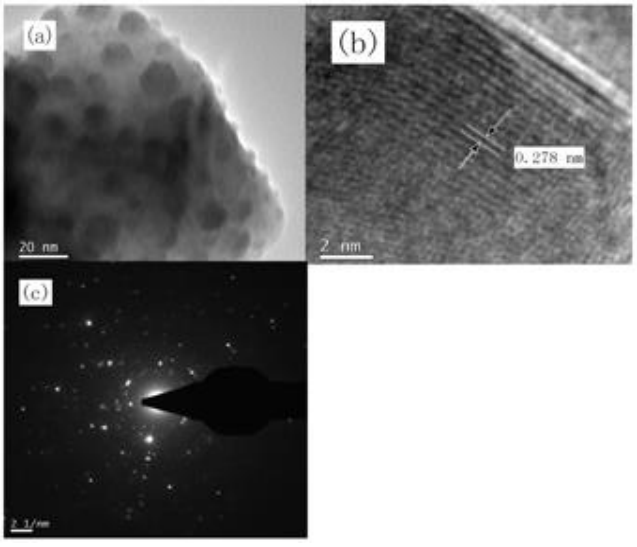

Fig. 3. (a) TEM image of the sample with La =10%, (b) its magnified image, (c). SAED patterns.

Fig. 4 shows the magnetization hysteresis (M–H) loops of $Bi_{1-x}La_xFeO_3$ (x=0.05, 0.10, 0.15, 0.20, 0.25) nanoparticles after extraction of the complementar antiferromagnetic signal at room temperature. All of them present ferromagnetism. An obvious magnetic hysteresis loop that can be observed for x = 0.05 indicates the incorporation of La^{3+} ions into the $BiFeO_3$ structure increases the magnetization. The magnetic moment of the samples is greatly improved with increasing La doping content in $BiFeO_3$. The saturation magnetization is increasing from 0.02 emu/g to 0.17 emu/g with the increasing from $Bi_{0.95}La_{0.05}$ to $Bi_{0.8}La_{0.2}FeO_3$ at room temperature. The magnetic moment of $Bi_{0.75}La_{0.25}FeO_3$ deviates from this trend and decreases to 0.16 emu/g as shown the inset (a) of Fig. 4. Similar ferromagnetic moment enhancement has been observed previously [22].

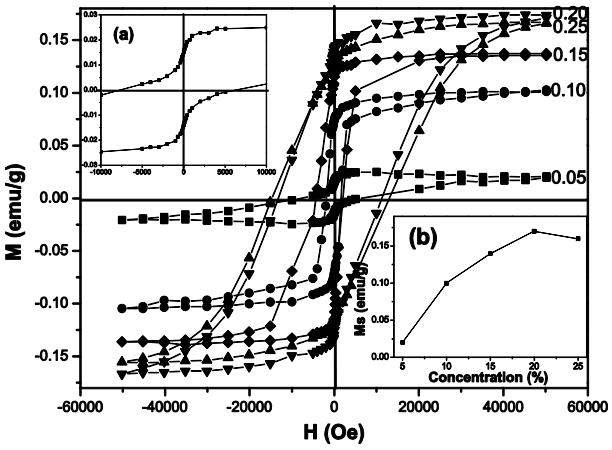

Fig. 4. Room temperature M-H curves for $Bi_{1-x}La_xFeO_3$ (x=0.05, 0.10, 0.15, 0.20, 0.25) nanoparticles. Inset: (a) the magnified view of the central region; (b) The variation of remanent magnetization as a function of La doping.

Several reasons contribute to the enhancement of ferromagnetism when the doped concentration is lower than x=0.2. Firstly, compared to bulk samples, the enhanced ferromagnetism may be interpreted by the uncompensated moment, which arises from the antiferromagnetism core and ferromagnetism surface of the nanoparticles. Secondly, La doping might have increased the canting angle, which in turn has resulted in enhanced magnetic properties. Finally, the spiral-modulated spin structure of $BiFeO_3$ is suppressed by the substitution of smaller La (1.06 Å) ions for Bi (1.20 Å) ions, which leads to the structural distortion from rhombohedral to orthorhombic, giving rise to an improved magnetization [23, 24].

The inset (a) of Fig. 4 shows a magnified view of the central region of the M-H loop obtained for $Bi_{0.95}La_{0.05}FeO_3$ sample. A shift in hysteresis loops of the sample toward negative field axis was observed. This shift is ascribed to exchange coupling between the ferromagnetic surface and antiferromagnetic core of the $BiFeO_3$ and La-doped $BiFeO_3$ nanoparticles that also support Neel's model of magnetization for antiferromagnetic nanoparticles [25].

In contrast to $Bi_{1-x}Gd_xFeO_3$ samples, where the alignment of the large own magnetic momentof Gd^{3+} ions (m = 8.0 μB,) gives rise to a colossal enhancement of the

magnetization with decreasing temperature or increasing external magnetic field, Fig. 5 shows the field-dependent magnetization of $Bi_{1-x}La_xFeO_3$ (x=0.05, 0.10, 0.15, 0.20, 0.25) nanoparticles at 5 K. The non magnetic of the La^{3+} ions has no significant influence on the low-temperature magnetic properties of the substituted compounds. A slight decrease in the magnetization taking place in a low-temperature range implies that the magnetic moments of La^{3+} ions tend to align anti-parallel with respect to a weak ferromagnetic component associated with the iron sublattice [26].

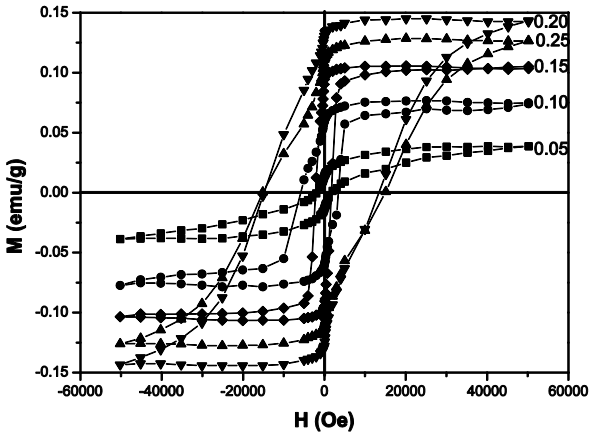

Fig. 5. M-H curves of $Bi_{1-x}La_xFeO_3$ (x=0.05, 0.10, 0.15, 0.20, 0.25) nanoparticles at 5K.

Fig. 6 shows the zero field cooled (ZFC) and field cooled (FC) curves of the $Bi_{0.9}La_{0.1}FeO_3$. For zero-field-cooled (ZFC) magnetization measurements, the sample was first cooled from room temperature down to 5 K in zero field. After applying the magnetic field of 1000 Oe at 5 K, the magnetization was measured in the warming cycle with field on. Whereas for field-cooled (FC) magnetization measurements, the sample was cooled in the same field (1000 Oe) down to 5 K, and the FC magnetization was measured in the warming cycle under the same field. We note that the ZFC and FC curves of samples start to split below about 270 K and a divergence between ZFC and FC magnetization curves increases with decrease in the temperature. The presence of a net magnetic moment for all the samples and the observation of a branching phenomenon between the FC and ZFC at $T \leq 270$ K is attributed to the non-compensation of surface spins. Néel proposed a model for antiferromagnetic nanoparticles based on the presence of two sublattices: one with spins up and another with spins down at the surface [27]. Any imbalance in the number of spins at the surface is the origin of a net magnetic moment in "antiferromagnetic" nanoparticles below the ordering temperature of spins.

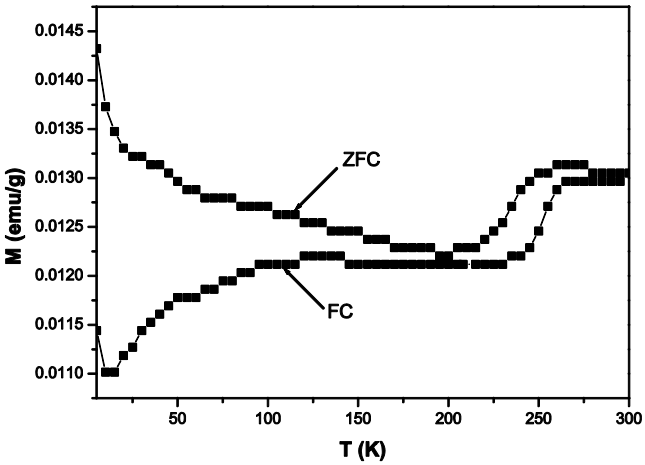

Fig. 6. ZFC/FC curves of $Bi_{0.9}La_{0.1}FeO_3$ nanoparticles from 5 K to 300 K.

4. Conclusions

In summary, $Bi_{1-x}La_xFeO_3$ (x=0.05, 0.10, 0.15, 0.20, 0.25) nanoparticles were prepared by simple sol-gel method. The effects of La content on the structure and ferromagnetic properties of these nanoparticles were investigated. Nanoparticles show gradual structural changes from rhombohedral towards a orthorhombic structure as the La content increases, also evident from disappearance of peak splitting upon increasing the doping level. The magnetization field curves showed that the magnetization strengthened with the increase of the La doped proportion ($0 \leq x \leq 20$) and weakened with the La doped proportion at x=0.25. La substitution at Bi site suppresses spiral spin modulation as well as increases the canting angle, which is believed to be the main cause to exhibit magnetic behavior at room temperature as well as low temperature (5 K). These results indicate that appropriate substitution of La is effective in enhancing the ferromagnetic properties of the $BiFeO_3$ nanoparticles.

Acknowledgments

The authors are grateful to Prof. Erqing Xie and Dr. Jiecai Fu of Lanzhou University for help with the TEM measurements.

References

[1] J. F. Scott, Nat. Mater. **6**, 256 (2007).
[2] J. Allibe, S. Fusil, K. Bouzehouane, C. Daumont, D. Sando, E. Jacquet, C. Deranlot, M. Bibes, A. Barthelemy, Nano Lett. **12**, 1141 (2012).
[3] M. Bibes, A. Barthelemy, Nat. Mater. **7**, 425 (2008).
[4] Y. Tokura, Science **312**, 1481 (2006).
[5] C. A. F. Vaz, J. Hoffman, C. H. Ahn, R. Ramesh, Adv.

Mater. **22**, 2900 (2010).
[6] P. Maksymovych, J. Seidel, Y. H. Chu, P. P. Wu, A. P. Baddorf, L. Q. Chen, S. V. Kalinin, R. Ramesh, Nano Lett. **11**, 1906 (2011).
[7] A. R. Damodaran, C. W. Liang, Q. He, C. Y. Peng, L. Chang, Y. H. Chu, L. W. Martin, Adv. Mater. **23**, 3170 (2011).
[8] A. Q. Jiang, C. Wang, K. J. Jin, X. B. Liu, J. F. Scott, C. S. Hwang, H. B. Lu, G. Z. Yang, Adv. Mater. **23**, 1277 (2011).
[9] Y. C. Chen, Q. He, F. N. Chu, Y. C. Huang, J. W. Chen, W. L. R. K. Vasudevan, V. Nagarajan, E. Arenholz, S. V. Kalinin, Y. H. Chu, Adv. Mater. **24**, 3070 (2012).
[10] B. Bhushan, D. Das, A. Priyam, N. Y. Vasanthacharya, S. Kumar, Mater. Chem. Phys. **135**, 144 (2012).
[11] P. Li, Y. H. Lin, C. W. Nan, J. Appl. Phys. **110**, 033922 (2011).
[12] I. Levin, M. G. Tucker, H. Wu, V. Provenzano, C. L. Dennis, S. Karimi, T. Comyn, T. Stevenson, R. I. Smith, I. M. Reaney, Chem. Mater. **23**, 2166 (2011).
[13] Z. L. Hou, H. F. Zhou, L. B. Kong, H. B. Jin, X. Qi, M. S. Cao, Mater. Lett. **84**, 110 (2012).
[14] S. K. Pradhan, B. K. Roul, AIP Conf. Proc. **320**, 1461 (2012).
[15] H. Naganuma, J. Miura, S. Okamura, Appl. Phys. Lett. **93**, 052901 (2008).
[16] J. G. Zhao, X. H. Zhang, S. J. Liu, W. Y. Zhang, Z. J. Liu, **557**, 120 (2013).
[17] B. L. Choudhary, S. Kumar, A. Krishnamurthy, B. K. Srivastava, AIP Conf. Proc. **1372**, 83 (2011).
[18] W. W. Hu, Y. Chen, H. M. Yuan, G. H. Li, Y. Qiao, Y. Y. Qin, S. H. Feng, J. Phys. Chem. C **115**, 8869 (2011).
[19] R. Haumont, J. Kreisel, P. Bouvier, F. Hippert, Phys. Rev. B **73**, 132101 (2006).
[20] G. L. Yuan, S. W. Or, H. L. Chan, J. Appl. Phys. **101**, 064101 (2007).
[21] C. Beekman, A. A. Reijnders, Y. S. Oh, S. W. Cheong, K. S. Burch, Phys. Rev. B **86**, 020403 (2012).
[22] Y. H. Lin, Q. H. Jiang, Y. Wang, C. W. Nan, L. Chen, J. Yu, Appl. Phys. Lett. **90**, 172507 (2007).
[23] K. Chakrabarti, K Das, B. Sarkar, S. K. De, J. Appl. Phys. **110**, 103905 (2011).
[24] Y. J. Zhang, H. G. Zhang, J. H. Yin, H. W. Zhang, J. L. Chen, W. Q. Wang, G. H. Wu, J. Magn. Magn. Mater. **322**, 2251 (2010).
[25] B. Bhushan, Z. X. Wang, J. Tol, N. S. Dalal, A. Basumallick, N. Y. Vasanthacharya, S. Kumar, D. Das, J. Am. Ceram. Soc. **95**, 1985 (2012).
[26] V. A. Khomchenko, V. V. Shvartsman, P. Borisov, W. Kleemann, D. A. Kiselev, I. K. Bdikin, J. M. Vieira, A. L. Kholkin, Acta Mater. **57**, 5137 (2009).
[27] D. P. Dutta, B. P. Mandal, R. Naik, G. Lawes, A. K. Tyagi, J. Phys. Chem. C **117**, 2382 (2013).

*Corresponding author: zhaojunliu@gmail.com
lynczjg@gmail.com